Design and performance analysis of extended wavelength InGaAs near-infrared photodetectors

2015 Jpn. J. Appl. Phys. 54 104301

(http://iopscience.iop.org/1347-4065/54/10/104301)

Japanese Journal of Applied Physics **54**, 104301 (2015) **REGULAR PAPER**
http://dx.doi.org/10.7567/JJAP.54.104301

Design and performance analysis of extended wavelength InGaAs near-infrared photodetectors

Jun Ma[1], Zhiwei Zhang[2*], Guoqing Miao[2], and Yuguang Zhao[1]

[1]*Key Laboratory of Automobile Materials, Ministry of Education, and Department of Materials Science and Engineering, Jilin University, Changchun 130022, China*
[2]*State Key Laboratory of Luminescence and Applications, Changchun Institute of Optics, Fine Mechanics and Physics, Chinese Academy of Sciences, Changchun 130033, China*
E-mail: zhangzw@ciomp.ac.cn

Received April 27, 2015; accepted August 13, 2015; published online September 18, 2015

In this work, we investigate the performance of InGaAs p–i–n photodetectors with cut-off wavelengths near 2.5 μm. The influences of different cap materials on the optoelectronic properties of InGaAs detector are also compared and discussed. The result indicates that the InAlAs used as cap layer can lead to lower dark current and larger quantum efficiency than other cap layers. In addition, our results show that the device performance is influenced by the valence band offset. This work proves that InAlAs/InGaAs/InP structure is a promising candidate for high performance detector with optimally tuned band gap. Furthermore, dark current mechanisms for extended wavelength InGaAs detectors are analyzed in-depth.

1. Introduction

In recent years, there are growing needs for 1–2.5 μm near-infrared detectors, the most important applications are spectral imaging, such as earth observation, remote sensing and environmental monitoring.[1,2] Varieties of near-infrared detectors have been developed. Compared with the conventional HgCdTe or antimonide materials, the InGaAs material has higher electron mobility, better stability, anti-radiation characteristic, mature growth, device processing technology, and performance of the detectors, especially in high operation temperature and high irradiation environment. InGaAs p–i–n detector has recently become one of the most important near-infrared detectors. However, narrow detection range and large dark current remain a major problem restricting its development and application. There is a strong need for high performance extended wavelength InGaAs detector at room temperature.

The response wavelength of ternary InGaAs can be well-regulated and shifted by changing the composition proportion. To shift the response of the detector to longer wavelength, the indium (In) content in the InGaAs should be increased. For instance, to move the cut-off wavelength of InGaAs detector grown on InP substrate from 1.7 to 2.5 μm, the In contents of InGaAs have to be increased from 53 to about 82%, which introducing a quite large lattice mismatch of about 2% between InGaAs layer and InP substrate. The number of dislocations and defects increases which will degrade the device performance. In this case, an extraordinary buffer layer should be inserted to prevent the propagation of threading dislocations and degradation of the material quality. Up to now, intensive research has been done on the growth technology and buffer structures.[3] Extended wavelength InGaAs detectors grown using metal–organic vapor phase epitaxy (MOVPE) or metal–organic chemical vapor deposition (MOCVD) or molecular beam epitaxy (MBE) methods with different type of buffer layers and hetero-junction structures have been reported. The experimental results clearly indicated that InGaAs detectors using InAsP buffer layers have been successfully fabricated with good opto-electronic properties.[4,5] The InAsP buffer seemed to perform better than InGaAs in terms of detector R_0A product and crystal quality, while linear grading in the buffer layer seemed to be better than step grading. Recent studies have showed a two-step growth method can effectively suppress the dislocations and defects extending to the epilayers, and improve the material quality.[6] Although their performances were well evaluated, the control of dark current still remains a challenge.[7] Other aspects for the improvement of the device will include the responsiveness and the extension of the operating wavelength range.

Since the main limitation for device performance is associated with device structure, the design of novel device structures is an effective way to improve detector performance. InP has been developed as cap material while InGaAs as absorbing material in the p–i–n structure for a long time. Due to the wide range of attainable band gap energy from 0.36 to 1.35 eV, InAsP materials are very important for photodiodes, high electron drift velocity devices, infrared emitting and detecting devices.[8,9] Compared to InP material, the lattice-matched InAsP with high electron mobility and small hole effective mass is a promising cap material which could be used in the field of near-infrared detection. In addition, high performance detector utilizing InAlAs as the cap material have been reported.[10] InAlAs has a better ionization coeffcient ratio than InP, which leads to both lower excess noise and higher gain-bandwidth product. Moreover, the temperature dependence of the ionization process in InAlAs is much smaller than that of InP. Therefore, InAsP and InAlAs lattice matched to InGaAs, seems more suitable than InP as cap material. However, to the best of our knowledge, few works about the effect of cap layer on extended wavelength InGaAs p–i–n detector performance have been reported so far. In addition, the detailed characteristics of high In content InGaAs detector, especially the dark current mechanism, have not been studied thoroughly. By increasing the In content of InGaAs, a quite large lattice mismatch between InGaAs epilayer and substrate is introduced and the dark current mechanism of the devices becomes complicated.[11] As the large lattice mismatch introduce a lot of trap states at the interface or in the absorption layer, the

Table I. Layer structure of the simulated photodetector.

Layer	Composition	Type	Thickness (μm)	Doping (cm^{-3})
Cap	$InP/InAs_{0.6}P_{0.4}/In_{0.82}Al_{0.18}As$	p	1	2×10^{17}
Absorption	$In_{0.82}Ga_{0.18}As$	n	3	8×10^{16}
Buffer	$InAs_yP_{1-y}$ ($y = 0$–0.6)	n	1	2×10^{18}
Substrate	InP	n	—	2×10^{18}

trap assisted tunneling current is proposed to be significantly increased and play an important role in the dark current of InGaAs with high In content.[12] Therefore, more research is needed on both device structure and dark current mechanism of InGaAs detector.

2. Modeling details

The device simulation was done using APSYS, which self-consistently solves the Poisson's equation, and current continuity equations for electrons and holes within drift-diffusion model by finite-element method.[13,14] In the simulations, the physical models includes optical absorption, photo-generated carrier drift and diffusion processes, Shockley–Read–Hall, Auger, and radiative recombination models. APSYS simulator is used to study the InGaAs detector, which has been widely utilized for analyze the device performance.[15] A good agreement among the experimental data and the theoretical values provides the basis for calculating the carrier density.[16] Thus, APSYS is a useful tool to access new designs or to optimize existing devices.

Simulated structure is a modification of conventional InGaAs p–i–n photodetector reported in experiment.[17] From top to bottom, the epitaxial layer structure consists of a heavily p-doped cap layer, a slightly n-doped $In_{0.82}Ga_{0.18}As$ adsorption layer, a linearly graded InAsP buffer layer, and InP substrate layer. The device structure parameters of the InGaAs p–i–n detector used in our simulation are given in Table I. Three types of cap layers, InP, InAsP, and InAlAs, were used in the simulation. For comparison, the identical simulation parameters were employed in all simulations. Performance characteristics such as dark current, photocurrent, responsivity and band diagram have been simulated at 300 K. Then, dark current mechanisms were analyzed according to current–voltage (I–V) curves at different temperatures. Analysis of the band diagrams can also provide basic information about design correctness and device properties.

3. Results and discussion

Different types of cap layers were used to investigate the effect of cap material on the performance and behavior of photodetectors. We tested the near-infrared detector with three types of cap layers: InP, InAsP, and InAlAs. The dependence cap material dependence of the dark I–V characteristics for InGaAs detector is shown in Fig. 1(a). The dark current behavior are different in the low and high reverse bias regions. In the reverse bias below 0.1 V, the dark current increases rapidly with the bias voltage and shows an athermal behavior. The dark current density of the InGaAs photodetector is about 100 μA/cm^2 at a reverse bias of 0.1 V. In the reverse bias above 0.1 V, the dark current in this region was

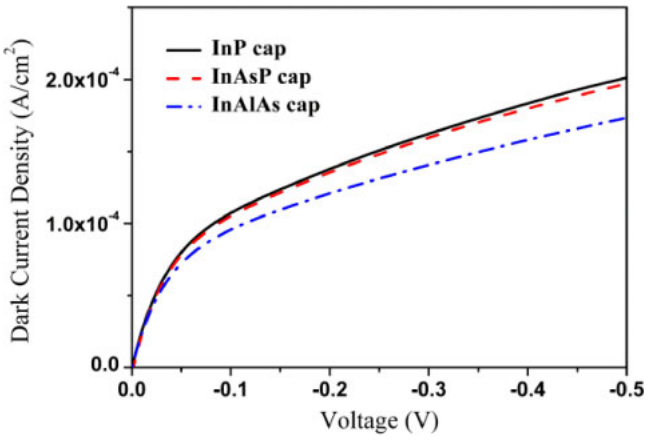

(a)

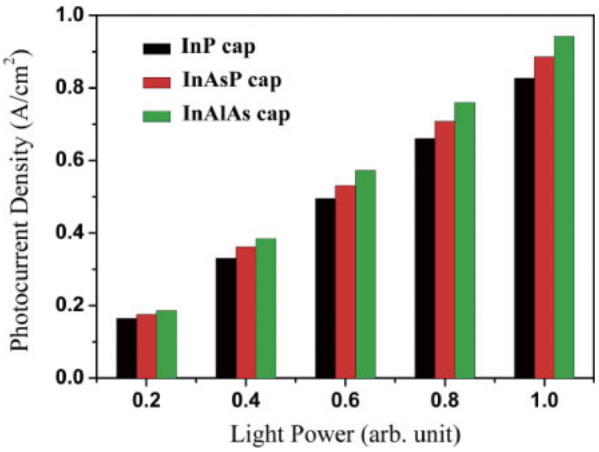

(b)

Fig. 1. (Color online) Dark current (a) and photocurrent (b) characteristics of InGaAs detectors with different cap layers at room temperature.

increased slowly with the bias, meanwhile a relative strong temperature dependent leakage current was observed.[18] At a reverse voltage of 0.5 V, the dark currents of about 201, 197, and 173 μA/cm^2 were obtained at 300 K, respectively. The dark currents of InAlAs cap detector are considerably smaller than for the InAsP and InP detector, especially at higher biases. The InP cap detector shows a larger dark current density at room temperatures. This may be because of the relatively larger dark current due to higher defect density. These defects provide midgap generation–recombination centers, increasing the generation–recombination current. Thus, our proposed InAlAs or InAsP cap detector exhibits lower dark current compared to the detector with InP cap. In addition, a smaller tunneling current is expected due to the slightly larger band gap of InAlAs than InAsP. The results showed that in the near-infrared region over 2.5 μm, the dark current of a detector is high, but when the same structure is placed within an optimally designed InAlAs cap, its dark current can be improved. Figure 1(b) shows the variation of photocurrent of different cap layers with input at room temperature. It can be noted that the photocurrent for InAlAs and InAsP cap layers were more than that for InP cap layer despite the fact that the band gap of InP is bigger. Two factors that could potentially contribute to the lower photocurrent for InP cap detectors are the phonon scattering effect of carriers in

the cap region and poor hole injection. It is clear that the defects in the mismatch material system have a much stronger scattering effect on the carriers. Therefore, using a InP material as the cap layer may cause more incident light absorption in the cap layer, because of the reduction of the incident light traversing the cap layer into absorption lower photocurrent in the structure. Additionally, hole injection efficiency is also nonnegligible. It is noteworthy that in the InP cap structure there is obvious potential barrier at the p-InP/i-InGaAs interface in the valence band (for holes). This is another harmful factor influencing the carrier collection efficiency. The rate that carriers leave the active region was faster in InAlAs or InAsP cap detector as compared to InP cap detector. Therefore, the probability of carrier recombination was decreased with higher photocurrent. Furthermore, InAlAs is used as cap layer, it is possible to passivate the surface of InGaAs material, which reducing the surface recombination probability of photo-generated carriers and thereby improve the quantum efficiency of device. It can be concluded that the optoelectronic properties of photodetector is manipulated not only by the thickness and material composition of the adsorption layers, but also by control of the kind of cap layer.

Relative spectral responses of the three detectors are shown in Fig. 2(a). The results show that the response wavelength range of the InGaAs detector is between 1 and 2.5 μm, and the responsivity varies with the wavelength. For three kinds cap detectors were measured as shown, the cut-off wavelength keeps unchanged whereas the response range widen obviously to about of the InP cap detector, which is determined by the band gap of cap and absorption layer material at room temperature. But the response of InAsP or InAlAs cap detector is more intensity than for the InP cap detector. This is due to the smaller band gap of the former materials which not only leads to an increased intrinsic carrier concentration affecting the photocurrent, but also leads to increased the response intensity. The order of responsivity values obtained by InAlAs cap model and those obtained by InAsP cap simulation was found to be very close. The InAlAs or InAsP cap devices exhibit very a high value of responsivity which was estimated to be of the order of 0.8 A/W. The results showed that the higher responsivity of photodetector can be attributed to their high charge carrier mobility. Compared to the device fabricated from the InP and InAsP cap layer, InAlAs cap did cause much change of the device performance. This meaning that there are better optoelectronic properties in the InAlAs cap and the performance are improved for InGaAs photodetectors. Based on aforementioned simulation results, we know that the InAlAs/InGaAs/InP detector is better than the other two detectors. Figure 2(b) shows the relative spectral response of the InAlAs/InGaAs/InP detector in the temperature range from 300 to 160 K. As the temperature decreases, the cut-off wavelength diminishes along the short-wave direction due to the increase of InGaAs band gap. The reduction of the response peak is less than 10% with the temperature decreases from 300 to 160 K. Such temperature dependent characteristics of the responsivity should be analyzed. For the extended wavelength InGaAs detector, the analytical model and simulation processes show that, the temperature dependent characteristics of the responsivity could be attributed to diversified

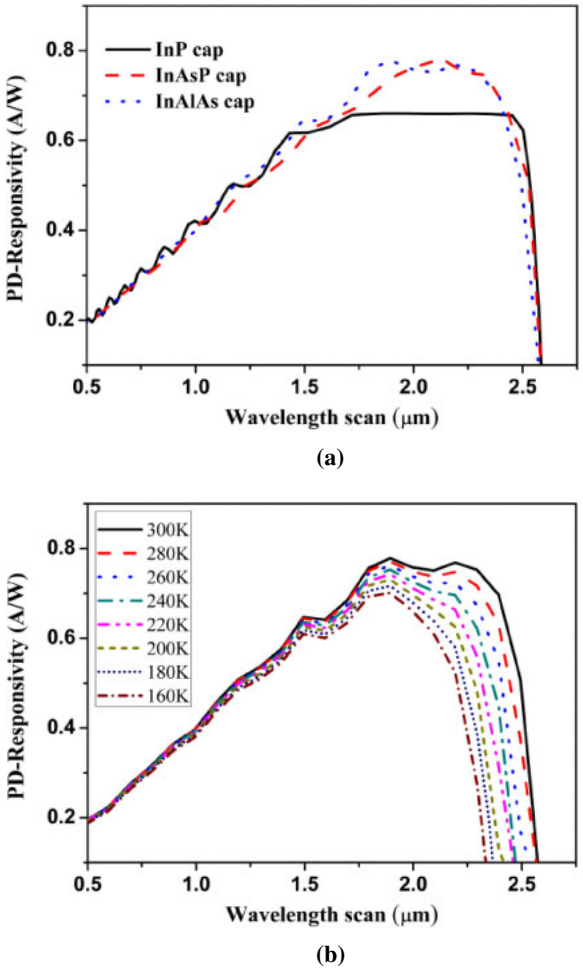

Fig. 2. (Color online) (a) Relative spectral response of InGaAs detectors with different cap layers at room temperature. (b) Relative spectral response of the InAlAs/InGaAs/InP detector at different temperatures from 300 to 160 K in step of 20 K.

reasons. The decrease of the operation temperature leads to a remarkable decreasing of the diffusion length of minority carriers. In certain operation wavelength region below the band gap, the absorption coefficient of the absorption layer also has a notable drop. These two factors result in a relatively strong positive temperature coefficient of response. Meanwhile, a slight increasing of the depletion width and diffusion coefficient leads to a quite weak negative temperature coefficient. With these competing effects, the total temperature coefficient of the responsivity is positive, and the most important factor is the diffusion length change of the minority carriers.

For better describing the role of cap layer, the detail energy band structures of the proposed three detectors are sketched in Fig. 3. Compared to the InP cap device, InAsP and InAlAs cap device have a small bandgap, which improves the limitation on the carrier transport, so as to enhance the response efficiency of detector. In addition, the valence band offset in the detector causes the increment in dark current. Because it can have a high valence band offset region at the interface, the InP cap detector may be more affected by misfit dislocations than the other two detectors with low offset region, which exhibit large dark current when significant numbers of such misfit dislocations intercept the interface

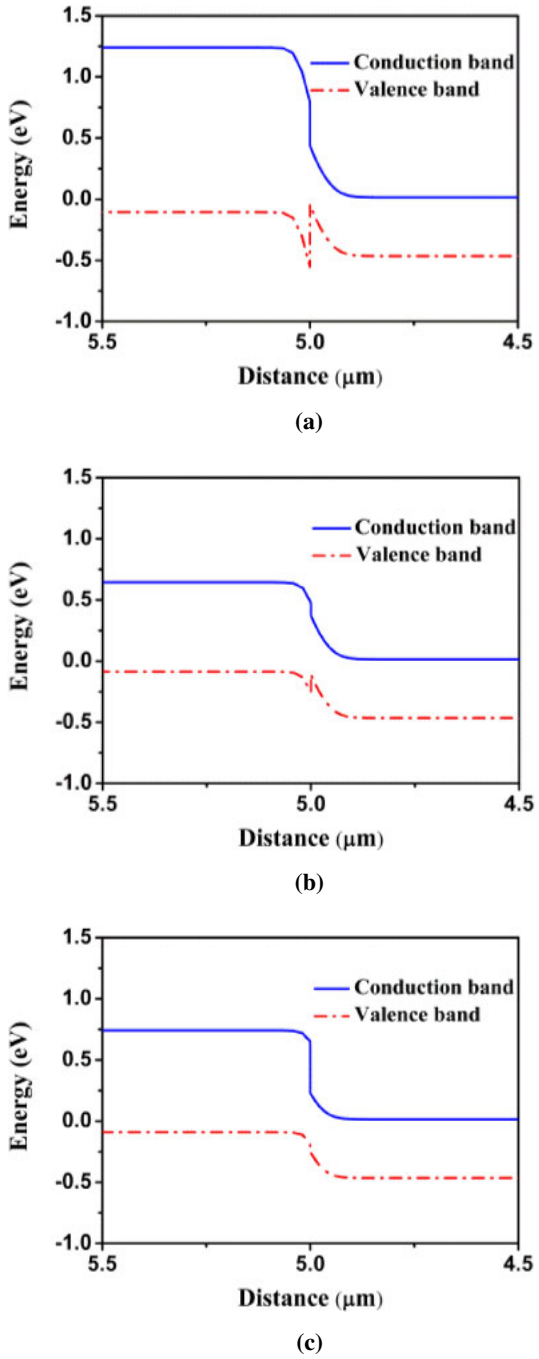

Fig. 3. (Color online) Energy band structures for the (a) InP/InGaAs, (b) InAsP/InGaAs, and (c) InAlAs/InGaAs heterojunctions at 300 K.

region. As discussed previously, the mismatch induce defects bring in additional energy levels within the band gap, which increases the recombination rate of minority carriers and majority carriers, and results in increased generation–recombination current. In contrast to the InP/InGaAs or InAsP/InGaAs heterojunction with a much larger valence band offset, the smaller valence band offset of InAlAs/InGaAs is more favorable for the low dark current operations. The band edges distribution across the heterostructure allows verification of the device architecture. Strong modification of band edge due to cap layer results for applying InAlAs material structure. A key enabling device design element is the band offset, which is used to implement the InGaAs near-infrared detector architecture for increasing the collection efficiency

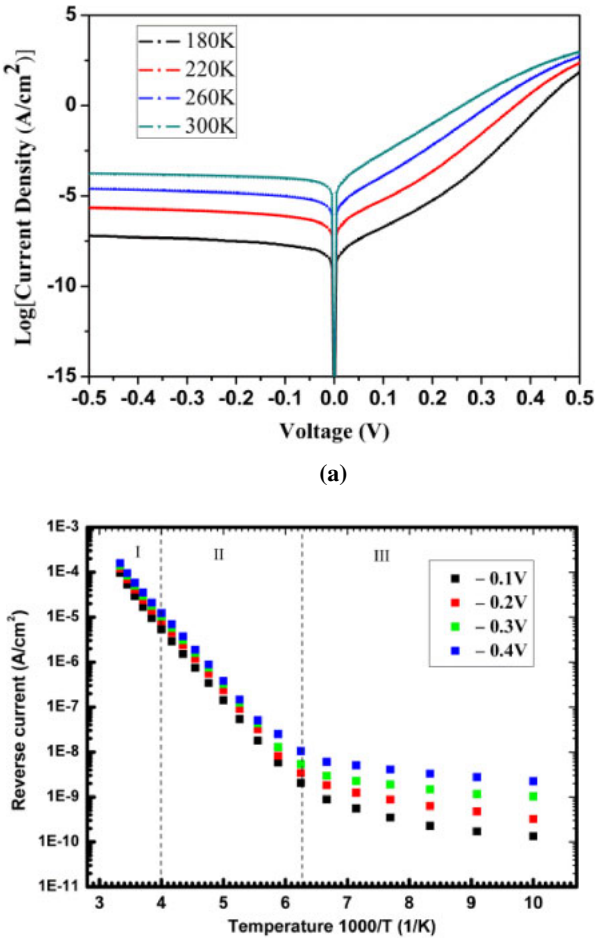

Fig. 4. (Color online) (a) Simulated dark current versus voltage for the InAlAs/InGaAs/InP detector at various temperatures. (b) Variation of dark current with temperature at various reverse bias.

of photo-generated carriers, and reducing dark current generation without impeding photocurrent flow. The valence band offset depends on the semiconductors and the amount of mismatch strain at the interface. The valence band offset induced barrier can be improved by making small adjustments to the device structure, through change in the design of InGaAs structure.

The dark current mechanisms of the devices are important for the photodetector application. Different dark current mechanisms have been reported by several groups. Li et al. recently reported that near zero-bias dark current of $In_{0.78}Ga_{0.22}As$/InP detectors is contributed from the diffusion mechanism.[19] Miao et al. proposed that both diffusion and generation–recombination currents are the dominate dark current contributors in $In_{0.82}Ga_{0.18}As$/InP detectors.[17] These results evidence considerable progress in the understanding of the matter. However, to date the dark current mechanism for the extended wavelength InGaAs detector remain elusive.[20] Further study is underway to find the origin of this dark current. Figure 4(a) shows the dark *I–V* curves of the InAlAs/InGaAs/InP detector at various temperatures. The dark current exhibits an exponential increase with the bias and has relatively strong temperature dependence. As the temperature decreases, the dark current of the device significantly decreased. The asymmetry of the dark *I–V*

curves shown in Fig. 4(a) is caused by the asymmetrical carrier injection from the bottom and top contact layers in different current directions. With the depletion of electrons from active layer, the electrons from contact layer become a dominant factor to influence the dark current. Under forward bias, more electrons are introduced from the bottom contact layer to the top contact layer because of the higher sheet electron density of the bottom contact layer, thus the dark current under reverse bias is lower than the forward bias condition. By increasing the forward bias, the shunt effect became negligible as the diffusion current exponentially increased with bias. It can also be seen that the dark current behaviors are different in the low and high reverse bias regions. The comparison between the different curves illustrated in Fig. 4(a) proves that dark current is dominated by diffusion and generation–recombination current in the low reverse bias. In addition, tunneling current is so small due to low bias that its contribution can be neglected.[21] In the high reverse bias, the dark current is nearly independent of bias, and is sensitive primarily to the recombination velocity at the interface. In fact, the effect of the tunneling process is also responsible for the dark current generation in these devices at high bias. To see the dark current generating mechanism more clearly, the dark current–temperature curves of the InAlAs/InGaAs/InP detector were shown in Fig. 4(b), measured at reverse bias 0.1, 0.2, 0.3, and 0.4 V. In the region "I", near room temperature, under different bias, the reverse dark current of the detector changed little, indicating that the dark current of detector is mainly composed of the diffusion current and generation–recombination current.[22] At higher temperatures, the dark current does not change significantly with the reverse bias, thus indicating that for higher temperatures the diffusion current dominates. This is because the diffusion current is a weak function of applied low reverse bias at higher temperatures. In the region "II", the dark current of detector with the temperature reduces at different bias and began to separate, making the sharp decline in the generation–recombination current and diffusion current, the tunneling current caused by the defects come into play.[23] In the region "III", the variation of detector dark current with temperature is very small and close to a constant, the diffusion current and generation–recombination current can be ignored, the dark current mechanism is the tunneling current.[12] As temperature decreases, the tunneling current decreases slightly, because the material band gap increases slightly (increasing the tunneling barrier). However, the tunneling current is not the only mechanism responsible for the flat behavior in the low temperature range. This phenomenon might result from surface leakage. Surface leakage is believed from abrupt termination of the periodic crystal structure, which creates a band bending on the sidewalls. This band bending causes electron accumulation or type inversion at sidewall surfaces, resulting in a conduction channel along sidewalls.[24] Therefore, through employing effective passivation technology, the surface leakage contribution stays lower in low temperatures, which can explain the fact that the tunneling current becomes domain dark current mechanism. In fact, diffusion current is the intrinsic parameter of the device and not controlled by the process level. Hence, the dark current in given device is the sum of the diffusion current and the current originated from the generation–recombination and from tunneling. At room temperature, the detectors are typically diffusion limited; then, as the temperature drops, generation–recombination mechanisms may dominate, and finally as the temperature drops even further, the dark current values reach a temperature independent asymptote often attributed to tunneling mechanism. While at low reverse bias, the generation–recombination current is the dominant contribution. And the tunneling current became significant only at high enough reverse bias. This supports the idea that the dominant source of dark current transitions from a more temperature sensitive mechanism (e.g., diffusion or generation–recombination) to a less temperature sensitive mechanism (e.g., tunneling) on increasing the reverse bias in the detector. As can be calculated based on the parameters extracted from Fig. 4, dark current of the photodetector is dominated by the generation–recombination current, which indicates that the deep traps at the bulk region, rather than the high-density surface traps, are the dominating factor for dark current. It is shown that deep traps may significantly affect the energy of the transport level especially at low temperatures. Deep traps essentially act as carrier recombination or trapping centers and adversely affect device performance. Relatively, there are more defects in the material InGaAs with higher In content due to lattice mismatch. These defects can introduce deep traps in the InGaAs bandgap that can emit electrons in the conduction band and holes in the valence band without the need for incident photons, leading to dark current generation. Lattice mismatch increases dark current and noise, limiting both dynamic range and sensitivity of a detector. The deep trap density get larger for longer cutoff wavelength devices due to the increasing lattice mismatch. This observation directly informs that reducing deep trap density can dramatically suppress the dark currents in the extended wavelength InGaAs detectors.

4. Conclusions

A novel design, InAlAs/InGaAs/InP structure, with a great potential for near-infrared detection was found in this research. After optimization, the dark current density can be reduced to 173 μA/cm^2 at a reverse bias of 0.5 V, while the wavelength can response up to 2.5 μm at room temperature. The results show that the performance of InGaAs detector strongly depend on the device structure, i.e., cap material. In addition, research results demonstrate that the valence band offset of heteojunction interface has important influence on the movement of carrier, which could result in changes of detector performance. The smaller valence band offset is more favorable for the low dark current operations. In the simulation the temperature dependence of the spectral response of $In_{0.82}Ga_{0.18}As$ detector has been analyzed and take into account. We also identify the contribution of each dark current mechanism at various temperatures, and found that the tunneling current became the dominant mechanism at low temperature.

Acknowledgements

This work is supported by the National Key Basic Research Program of China (No. 2012CB619201), and the Jilin Provincial Science and Technology Department (No. 20140520117JH).

1) R. W. M. Hoogeveen, R. J. van der A, and A. P. H. Goede, Infrared Phys. Technol. **42**, 1 (2001).
2) K. F. Zhang, H. J. Tang, X. L. Wu, Y. F. Li, T. Li, X. Li, and H. M. Gong, Semicond. Sci. Technol. **24**, 015008 (2009).
3) Z. C. Zhang, S. Y. Yang, F. Q. Zhang, B. Xu, Y. P. Zeng, Y. H. Chen, and Z. G. Wang, J. Cryst. Growth **247**, 126 (2003).
4) L. Ji, S. L. Lu, Y. M. Zhao, M. Tan, J. R. Dong, and H. Yang, J. Cryst. Growth **363**, 44 (2013).
5) X. Liu, H. Song, G. Miao, H. Jiang, L. Cao, X. Sun, D. Li, Y. Chen, and Z. Li, Solid State Commun. **151**, 904 (2011).
6) L. Zimmermann, J. John, S. Degroote, G. Borghs, C. Van Hoof, and S. Nemeth, Appl. Phys. Lett. **82**, 2838 (2003).
7) Y. W. Chen, W. C. Hsu, R. T. Hsu, Y. H. Wu, and Y. J. Chen, Jpn. J. Appl. Phys. **42**, 4249 (2003).
8) M. A. Meeker, B. A. Magill, T. R. Merritt, M. Bhowmick, K. McCutcheon, G. A. Khodaparast, J. G. Tischler, S. McGill, S. G. Choi, and C. J. Palmstrøm, Appl. Phys. Lett. **102**, 222102 (2013).
9) M. D. Birowosuto, A. Yokoo, G. Q. Zhang, K. Tateno, E. Kuramochi, H. Taniyama, M. Takiguchi, and M. Notomi, Nat. Mater. **13**, 279 (2014).
10) T. Nakata, J. Ishihara, K. Makita, and K. Kasahara, IEEE Photonics Technol. Lett. **21**, 1852 (2009).
11) Y. Gu, K. Wang, C. Li, X. Fang, Y. Y. Cao, and Y. G. Zhang, J. Infrared Millimeter Waves **30**, 481 (2011).
12) S. R. Forrest, M. DiDomenico, R. G. Smith, and H. J. Stocker, Appl. Phys. Lett. **36**, 580 (1980).
13) C. R. Anderson, J. Comput. Phys. **228**, 4745 (2009).
14) O. Marquardt, S. Boeck, C. Freysoldt, T. Hickel, S. Schulz, J. Neugebauer, and E. P. O'Reilly, Comput. Mater. Sci. **95**, 280 (2014).
15) H. P. Pan, A. Beling, H. Chen, and J. C. Campbell, Opt. Quantum Electron. **40**, 41 (2008).
16) D. Y. Lin, M. C. Wu, H. J. Lin, and W. L. Chen, Physica E **40**, 1380 (2008).
17) G. Q. Miao, T. M. Zhang, Z. W. Zhang, and Y. X. Jin, CrystEngComm **15**, 8461 (2013).
18) J. G. Chang, C. B. Wu, X. L. Ji, H. W. Ma, F. Yan, Y. Shi, and R. Zhang, Chin. Phys. Lett. **29**, 058501 (2012).
19) C. Li, H. Li, Y. Y. L. K. Wang, Y. Gu, and Y. G. Zhang, Semicond. Optoelectron. **6**, 807 (2009).
20) X. L. Ji, B. Q. Liu, Y. Xu, H. J. Tang, X. Li, H. M. Gong, B. Shen, X. L. Yang, P. Han, and F. Yan, J. Appl. Phys. **114**, 224502 (2013).
21) A. D. D. Dwivedi, A. Mittal, A. Agrawal, and P. Chakrabarti, Infrared Phys. Technol. **53**, 236 (2010).
22) Y. L. Zhao, D. D. Zhang, L. Qin, Q. Tang, R. H. Wu, J. J. Liu, Y. P. Zhang, H. Zhang, X. H. Yuan, and W. Liu, Opt. Express **19**, 8546 (2011).
23) S. R. Forrest, R. F. Leheny, R. E. Nahory, and M. A. Pollack, Appl. Phys. Lett. **37**, 322 (1980).
24) G. Chen, E. K. Huang, A. M. Hoang, S. Bogdanov, S. R. Darvish, and M. Razeghi, Appl. Phys. Lett. **101**, 213501 (2012).